CRYSTAL GROWTH & DESIGN
2009
VOL. 9, NO. 7
3052–3061

Selective Crystallization of the Metastable Anhydrate Form in the Enantiotropic Pseudo-Dimorph System of L-Phenylalanine using Concentration Feedback Control

Nicholas C. S. Kee,[†,‡,§] Paul D. Arendt,[†] Reginald B. H. Tan,[‡,§] and Richard D. Braatz*[,†]

University of Illinois at Urbana-Champaign, 600 South Mathews Avenue, Urbana, Illinois 61801, Department of Chemical and Biomolecular Engineering, National University of Singapore, 4 Engineering Drive 4, Singapore 117576, and Institute of Chemical and Engineering Sciences, 1 Pesek Road, Jurong Island, Singapore 627833

Received June 19, 2008; Revised Manuscript Received March 24, 2009

ABSTRACT: A batch recipe for the selective crystallization of the metastable anhydrate form of an enantiotropic pseudo-dimorph system, L-phenylalanine, in a mixed solvent system (75 wt % water and 25 wt % 2-propanol) was implemented by controlled tracking of a designed trajectory in the phase diagram. The solubility curves of both the anhydrate and monohydrate forms were determined using attenuated total reflection-Fourier transform infrared (ATR-FTIR) spectroscopy, coupled with chemometrics. Laser backscattering (focused beam reflectance measurement, FBRM) was used to determine the seeded metastable limit with the nucleated forms identified using in situ video microscopy. Batch operations seeded with the anhydrate form were implemented following various preset supersaturation profiles using concentration feedback control which regulated the cooling rate based on in situ measurement of the solute concentration. Undesired secondary nucleation at the metastable limit provided the operating constraints in terms of the maximum allowable supersaturation. Batch crystallization implemented at low constant absolute supersaturation with respect to the unwanted monohydrate form was successful in preventing cross nucleation and in selectively growing large anhydrate crystals with relatively uniform size. This methodology extended the useful range of the phase diagram to temperatures below the transition point, where the anhydrate form is metastable, to increase product yield compared to operations utilizing only the temperature range above the transition temperature, where the anhydrate form is stable.

Introduction

Many pharmaceutical compounds exhibit polymorphism,[1] the ability of a compound to adopt more than one crystal structure, or pseudo-polymorphism, the crystallization of solvates in which solvent molecules are incorporated into the crystal structure at well-defined lattice positions. Different polymorphs or pseudo-polymorphs can have vastly different product characteristics such as bioavailability and shelf-life. Hence, substantial effort is devoted to the design of consistent and reliable processes for producing the targeted polymorph or pseudo-polymorph to achieve reproducible therapeutic benefits and for regulatory compliance. Recipes for batch crystallization of a selected polymorph or pseudo-polymorph are typically designed by trial-and-error experimentation. A recipe could alternatively be obtained by optimization of a population balance model with solubilities and kinetics for the specific system obtained from a succession of D-optimal crystallization experiments,[2−4] but this approach can be time-consuming for complex polymorphic/pseudo-polymorphic systems (for a dimorphic system, this typically involves determining a half dozen expressions for nucleation, growth, and dissolution and a dozen or more kinetic parameters). The temperature range for phase transformation depends on the solvent composition, and so the crystal form can sometimes be selected by changing the solvent composition and/or by employing a different organic solvent.[5−9] There are also many papers on techniques for selective crystallization of metastable crystals, for example, by using critical seed loading,[10] fines dissolution,[11] additives,[12,13] sonication,[14] or microemulsions.[15] The implementation may be system specific. Strategies based on the solubility diagrams present a generic approach,[16−21] which focuses on the occurrence domains[22] of specific polymorphs. This approach for selective crystallization is based on seeding locations or spontaneous nucleation of the targeted form in these domains and controlling the cooling or antisolvent addition rate so that the combined effects of desaturation due to nucleation and crystal growth and supersaturation due to cooling or antisolvent addition do not drive the solute concentration into the domains of spontaneous nucleation of undesired forms.[17−20] Figure 1 shows schematics for enantiotropic dimorph systems with different metastable limits encountered during cooling (similar schematics apply in antisolvent crystallization). Form I, which is stable above and metastable below the transition temperature, can be selectively produced by operating from x to y - an undersaturated solution at x is cooled, seeded with Form I crystals after crossing the solubility curve for Form I, $C_{sat,I}$, and cooled with the supersaturation profile below the solubility curve of Form II, $C_{sat,II}$, to y.[17,20] Such operations have limited yield due to the restricted operating concentration range. If the metastable limit is known, the operating concentration range can be extended (with correspondingly increased yield) from x to z by operating the crystallizer such that the supersaturation is below the metastable limit[17] to avoid uncontrolled nucleation events.

Because experimentally establishing the metastable limit for each form is very difficult for many systems,[23] the diagrams in Figure 1 show a single metastable limit, which is defined as the point of uncontrolled nucleation regardless of form. The metastable limit should be measured in the presence of seed crystals, as this is the most appropriate for defining the maximum supersaturation for seeded operations.[51] The form produced at the metastable limit is generally dependent on the solvent type, temperature range, and seed form. These operating pathways for preferential crystallization of the mestastable form

* Corresponding author. Phone: 217-333-5073. Fax: 217-333-5052. E-mail: braatz@uiuc.edu.
[†] University of Illinois at Urbana-Champaign.
[‡] National University of Singapore.
[§] Institute of Chemical and Engineering Sciences.

10.1021/cg8006537 CCC: $40.75
Published on Web 05/14/2009

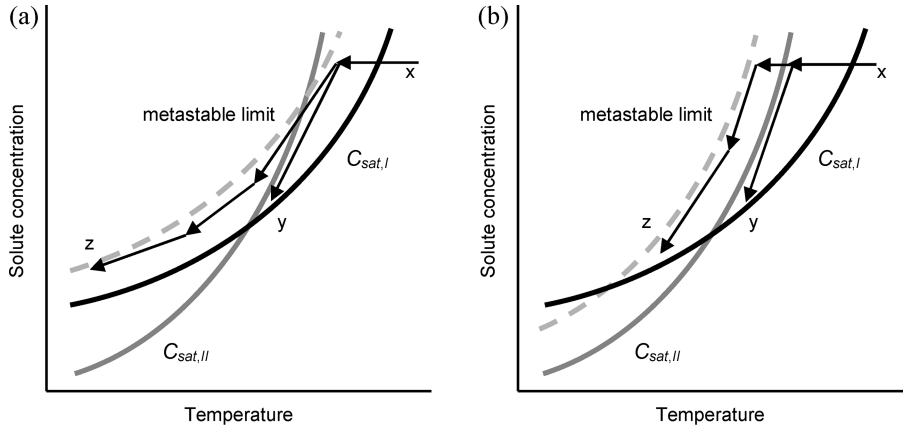

Figure 1. Schematic of various selective crystallization operations for Form I, in an enantiotropic dimorph system based on the solubility diagram and depending on the location of the metastable limit: (a) and (b) have metastable limits that parallel the solubility curves for forms I and II, respectively.

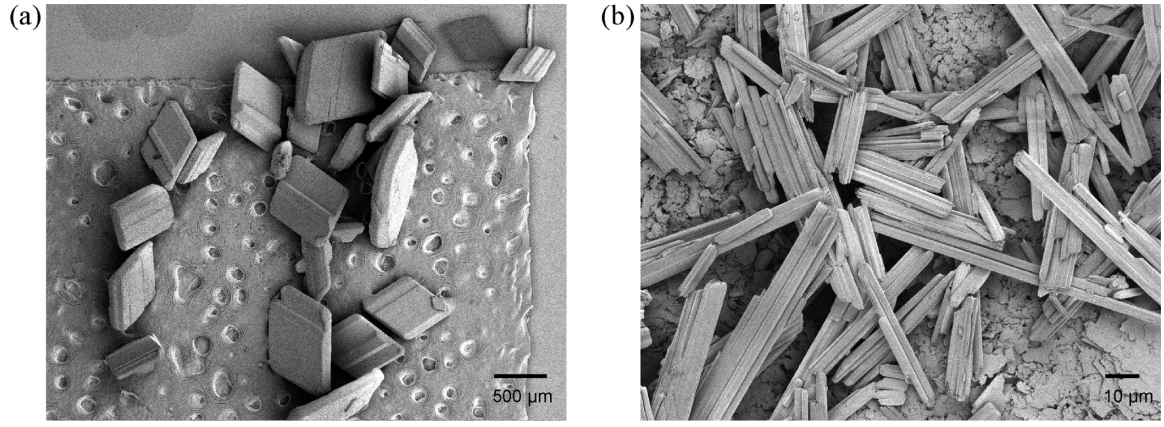

Figure 2. Scanning electron micrographs of L-phe crystals: (a) anhydrate form, (b) monohydrate form.

are not exhaustive; however, this methodology presents a systematic and generic approach, based on the solubility and metastable limit diagram that can be expected to hold for a wide variety of crystal−solvent systems. Central to the implementation of such operations is concentration feedback control[24−28] of the cooling or antisolvent addition rate to balance the desaturation due to crystallization with increased supersaturation caused by cooling or other means to follow the desired supersaturation profile. In concentration feedback control, the controller compares the solute concentration to some preset supersaturation, and adjusts the cooling or antisolvent addition rate accordingly so that the preset supersaturation curve is followed.[25,27,28] The robustness of this approach to most variations in growth and nucleation kinetics and most practical disturbances has been demonstrated for both cooling and antisolvent crystallizations in non-polymorphic systems.[16,28−30] More recently, this has been applied to the selective crystallization of the metastable α-form crystals in the monotropic dimorph system of L-glutamic acid.[31]

L-Phenylalanine (L-Phe), an enantiotropic pseudo-dimorph system, exists in two different crystalline forms: the anhydrate form, which appears as rhombic platelets, and the needle-like monohydrate form (Figure 2), previously denoted as β- and α-forms,[15,32] respectively. This paper describes the application of the concentration feedback control methodology for the pseudo-dimorph system of L-phe in a mixed solvent system consisting of water and 2-propanol with the objective of selectively crystallizing the anhydrate form in a seeded system to a temperature below the transition point, where this form is metastable. The lower and upper bounds of the operating regime are specified by the anhydrate form solubility curve and metastable limit, respectively.

Attenuated total reflection-Fourier transform infrared (ATR-FTIR) spectroscopy coupled with a calibration model constructed using chemometric techniques[33,34] was used to provide in situ solute concentration measurements. Focused beam reflectance measurement (FBRM), which measures in situ characteristics of crystal size distribution, was used to detect the metastable limit.[27,35,36] In situ video microscopy was used to assess the nucleated form. The seeded batch cooling crystallizations were implemented with concentration feedback control at different supersaturation profiles to determine an appropriate recipe for selectively growing anhydrate L-Phe crystals.

Experimental Procedures

Materials and Instrumentation. A Dipper-210 ATR immersion probe (Axiom Analytical) with ZnSe as the internal reflectance element attached to a Nicolet Protégé 460 FTIR spectrophotometer was used to obtain the spectra of the L-Phe solution. Sixty-four scans were used to compute each FTIR spectrum. The total particle counts per second of the crystals in solution was measured every 30 s using Lasentec FBRM with version 6.0b12 of the FBRM Control Interface software. In addition, in situ images of the slurry were obtained using Lasentec particle vision and measurement (PVM). The solution temperature was controlled by ratioing hot and cold water to the jacket with a control valve as described previously,[27] and was measured every 2 s using a Teflon-coated thermocouple attached to a Data Translation 3004 data acquisition board via a Fluke 80TK thermocouple module. Powder X-ray diffraction (PXRD) patterns of L-Phe crystals were collected offline using the Bruker general area detector diffraction system (GADDS, Bruker AXS, Inc.) with Cu $K_{\alpha 1}$ and Cu $K_{\alpha 2}$ (weighted sum) radiation and a step size of 0.02°. The anhydrate form is orthorhombic,

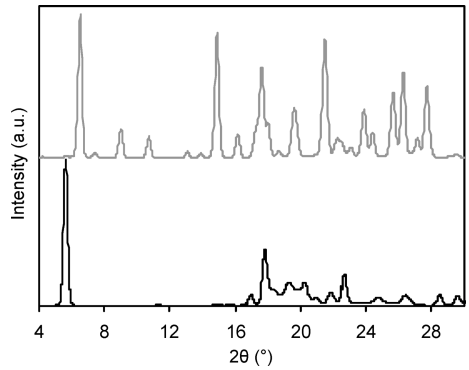

Figure 3. PXRD patterns of anhydrate (bottom) and monohydrate (top) forms of L-Phe.

while the monohydrate form is monoclinic; the space group is $P222_1$ for both.[13,32] The characteristic peaks of the PXRD patterns of both forms are consistent with that reported previously.[13] The characteristic peaks for the anhydrate form are at 5.54°, 22.70°, 28.40°, and 34.24°, while that for the monohydrate form are at 6.38°, 8.90°, 14.76°, and 27.70° (Figure 3). L-Phe crystals obtained commercially (>98.5%, Sigma Aldrich) were verified using PXRD to be pure anhydrate form.

Recrystallized anhydrate crystals were used in the metastable limit and batch crystallization experiments as seeds with a well-defined rhombic shape as opposed to the commercially available crystals, which were irregular platelets. The recrystallization procedure involved cooling initially undersaturated solution (0.030 g/g of mixed solvent) from 50 to 42 °C, then adding monohydrate crystals (the mixed solvent was 75 wt % deionized water and 25 wt % 2-propanol (ACS grade, Sigma Aldrich)). The solvent-mediated transformation of the monohydrate to the anhydrate form was completed after about 2.5 h under isothermal conditions and constant stirring. The PXRD pattern of the recrystallized anhydrate form was identical to that obtained commercially indicating that the recrystallized form was the same polymorph with a different crystal habit. The monohydrate form was produced by rapidly cooling an initially undersaturated solution (0.045 g/g of deionized water) from 60 to 25 °C where the monohydrate form is the most stable. The solid was filtered and dried following the procedures previously outlined,[13] in which the drying process did not result in dehydration. Similar rapid cooling procedures using the mixed solvent also resulted in the crystallization of the monohydrate form, which was likewise verified using PXRD. Scanning electron microscopy (SEM) samples were sputtered with 4−8 nm of Au/Pd before being recorded with a JEOL 7000F SEM.

Calibration for Polymorph Composition using PXRD. PXRD patterns of the powdered samples of L-Phe crystals with different polymorph compositions prepared using a mortar and pestle were used to create a calibration for polymorph composition (Figure 4). A linear calibration line was constructed by plotting the peak intensity ratio (6.38° and 8.90° for the monohydrate; 5.54° and 28.40° for the anhydrate form) against the mass ratio.

Table 1. PXRD Calibration Samples for Polymorph Composition

calibration sample	mass fraction (wt% monohydrate)	estimated mass fraction (wt% monohydrate)
1	0.00	0.00
2	0.00	1.12
3	0.00	0.00
4	20.1	22.4
5	20.1	24.3
6	40.3	39.7
7	40.3	42.9
8	60.5	61.7
9	60.5	54.6
10	80.7	80.3
11	80.7	81.3

Table 2. ATR-FTIR Calibration Samples for Solute Concentration Measurement

calibration sample	solute concentration (g/g solvent)	temperature range (°C)	number of spectra
Cs1	0.01503	29.0−19.1	16
Cs2	0.01903	34.0−20.1	22
Cs3	0.02303	42.1−22.0	31
Cs4	0.02700	47.9−32.8	24
Cs5	0.03103	54.0−37.2	27

Calibration for Solute Concentration. Different solute concentrations of L-Phe (Table 2) in the mixed solvent (400 g, 75 wt % deionized water and 25 wt % 2-propanol) were placed in a 500-mL jacketed round-bottom flask and heated until all the crystals dissolved. An overhead mixer was used to agitate the solution with a stirring speed of 175 rpm. The solution was cooled at 0.5 °C/min, while the IR spectra were collected until crystals started to appear. The IR spectra in the range 1100−1650 cm^{-1} were used to construct the calibration model. Figure 5 compares representative IR spectra of L-phe solutions used for calibration and the resulting regression coefficients. The calibration model relating the IR spectra and temperature to solute concentration was determined using various chemometrics methods.[37−39] The calculations used in-house MATLAB 5.3 (Mathworks, Inc.) code except for partial least squares (PLS) regression, which used the PLS Toolbox 2.0. The mean width of the prediction interval was used as the criterion to select among calibration models. The forward selection PCR 2 (FPCR 2) method[40] with a noise level of 0.001 gave the smallest prediction interval (±0.00034 g/g of solvent) which was compatible with the deviation of the experimental data points from the fitted solubility curves. The resulting calibration model had the form

$$C = \sum_{j=1100}^{1650} w_j a_j + w_T T + w_0 \qquad (1)$$

where C is the solute concentration (g/g solvent), a_j is the absorbance at frequency j cm^{-1}, T is the temperature (°C), and w_i, w_T, and w_0 are regression coefficients.

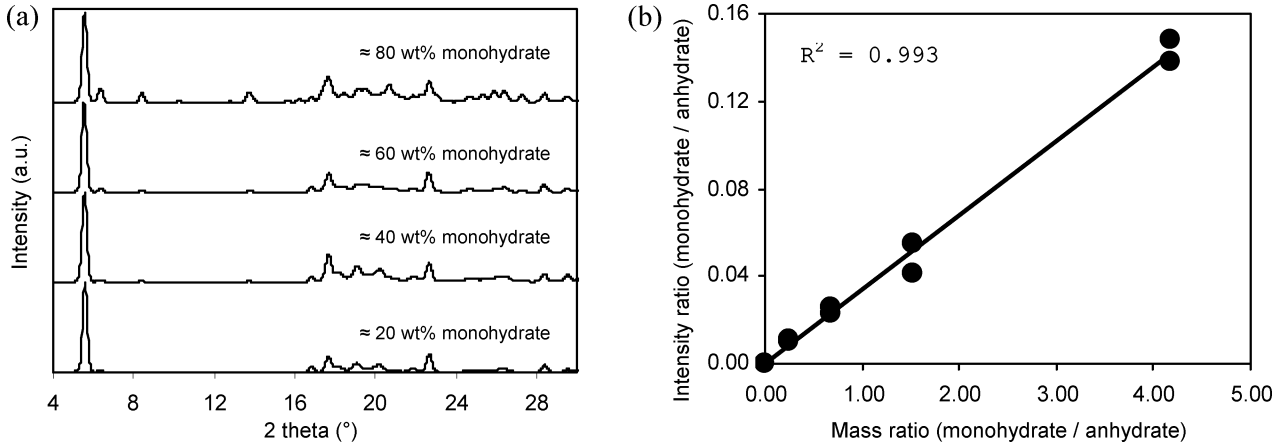

Figure 4. (a) PXRD patterns of calibration samples (the largest peak at $2\theta \approx 5.54°$ was normalized to the same value in all the patterns to better illustrate the variation in the characteristic peaks of the monohydrate form), (b) PXRD calibration line for polymorph composition.

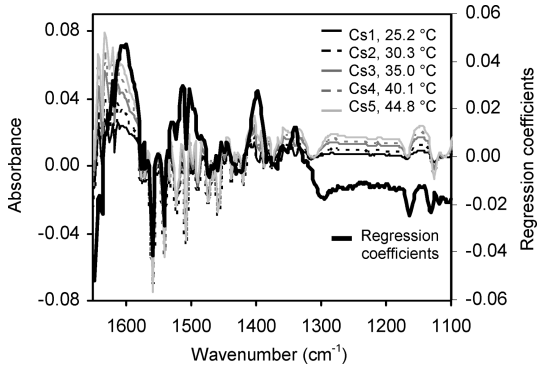

Figure 5. Representative ATR-FTIR spectra of the calibration samples and regression coefficients of the calibration model relating absorbance to solute concentration (regression coefficients for the temperature and the intercept are not shown).

Table 3. Initial Solute Concentrations in the Metastable Limit Experiments

run	initial solute concentration (g/g of solvent)
1m	0.01697
2m	0.01900
3m	0.02097
4m	0.02299
5m	0.02501

Table 4. Fitting Parameters for Anhydrate and Monohydrate Form L-Phe Solubility Curves

fitting parameters	anhydrate form	monohydrate form
$b_{0,i}$	6.351×10^{-3}	5.866×10^{-3}
$b_{1,i}$	2.218×10^{-4}	9.474×10^{-5}
$b_{2,i}$	7.502×10^{-6}	1.299×10^{-5}

Solubility and Metastable Limit Measurements. For each form, the IR spectra of L-Phe slurries were collected at different temperatures while equilibrating for 30 min to an hour, with solute concentration determined using the aforementioned calibration model. The time needed for equilibration was determined from the point when the total number of particles counted per second measured by FBRM remained constant (within the measurement noise). Care was taken to ensure that the slurry of monohydrate crystals contained only a small amount of excess solids, to prevent significant solid-phase interference on the IR measurements. Such interference may occur when the crystal dimensions are comparable to the penetration depth of the IR energy field, particularly in slurries with high solids density.[41,42] The measurements were performed twice for each evaluated temperature point. The monohydrate form solubility was also evaluated in a second method in which an equilibrated slurry of monohydrate form crystals was heated very slowly at 0.1 °C/min. The heating rate was sufficiently slow relative to dissolution that equilibrium was always maintained as the temperature increased. The saturation temperature and the corresponding solute concentration were determined at the lowest temperature (at the earliest time point) in which the concentration and particle counts/sec profiles approached a constant value, indicating complete dissolution.

The metastable limit of L-Phe solutions was determined for various initial solute concentrations (Table 3) using the polythermal method.[43] Each solution was heated above its saturation temperature to dissolve all crystals before cooling at 0.1 °C/min. As the main crystallization experiments utilized seeding, the metastable limit was determined for the seeded system; anhydrate crystals (0.50 g, 220−520 μm) were added at 0.6 °C after the solution temperature crossed the saturation temperature for the anhydrate form. Upon seeding, PVM images were collected to check for the appearance of the monohydrate needles and the crystals were monitored using FBRM. The start of a sharp increase in the particle counts/s some time after seeding was considered to be a nucleation event. In both the solubility and metastable limit experiments, the solvent mass and composition and the stirring speed of the overhead mixer were similar to that for calibration.

Seeded Batch Crystallization. Appropriate amounts of L-Phe and 400 g of the mixed solvent were heated to above the saturation temperature of the anhydrate form to create an undersaturated solution

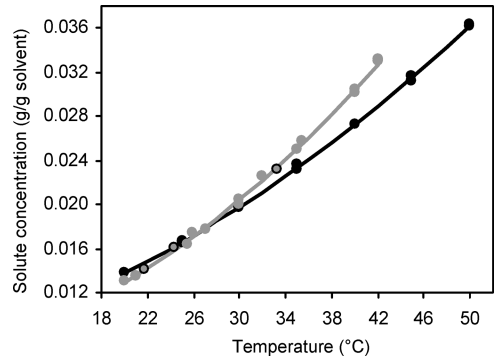

Figure 6. Solubility curves of L-Phe: $C_{sat,a}$ (•) and $C_{sat,m}$ (gray solid circles) in mixed solvent from isothermal studies, $C_{sat,m}$ (black circles with gray center) in mixed solvent from slow heating.

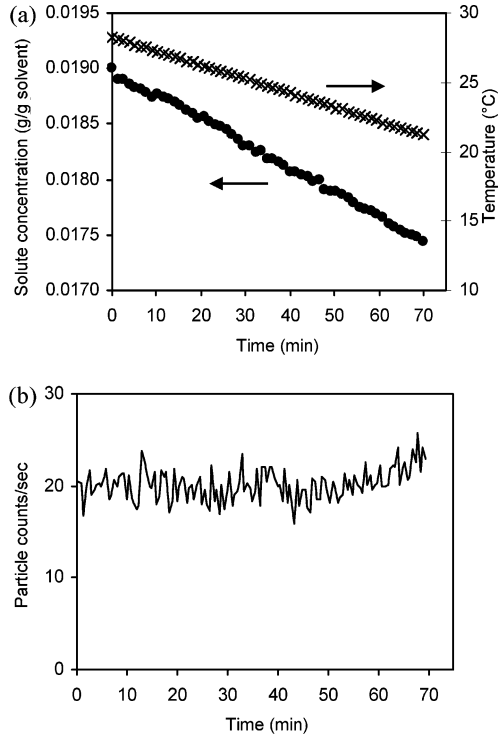

Figure 7. Run 2m experimental profiles with seeding at 0 min: (a) solute concentration and temperature, (b) particle counts/s.

with solute concentration 0.023 g/g of solvent. The solvent composition and the stirring speed were the same as that used for calibration. The solution was then cooled at 0.1 °C/min to 0.6 °C below the saturation temperature of the anhydrate form upon which anhydrate seed crystals with similar size distribution as that in the metastable limit experiments were added. The seed mass (0.51, 0.49, and 0.46 g for Runs 1, 2, and 3, respectively) represented an average seed loading of ~15% based on the expected yield; using a lower seed loading led to very noisy FBRM data, which would have reduced the ability to track nucleation during the experiments. Preset supersaturation profiles were followed during crystallization using concentration feedback control[27,28] to adjust the cooling rate accordingly based on in situ solute concentration measurements. The control algorithm was started shortly after seeding. Supersaturation set point profiles were selected at different constant absolute supersaturation ($\Delta C_i = C - C_{sat,i}$) with respect to both the anhydrate and monohydrate forms where $C_{sat,i}$ denotes the solubility (g/g of solvent) of the ith form, either the anhydrate (a) or monohydrate (m).

Results and Discussion

Solubility and Metastable Limit Measurements. The solubility curves for both forms of L-Phe in the mixed solvent were fit to

$$C_{\mathrm{sat},i} = b_{0,i} + b_{1,i}T + b_{2,i}T^2 \qquad (2)$$

(see Table 4 and Figure 6). The maximum deviation of the experimental data points from the fitted solubility curves (0.00031 and 0.00034 g/g of solvent for the anhydrate and monohydrate forms, respectively) were within the prediction intervals. The solubility measurement of the metastable form (i.e., anhydrate and monohydrate forms below and above the transition temperature, respectively) using the above methods applies when its dissolution is significantly faster than its transformation to the stable form, as is the case of L-Phe for the studied temperature range. The solubility of the monohydrate

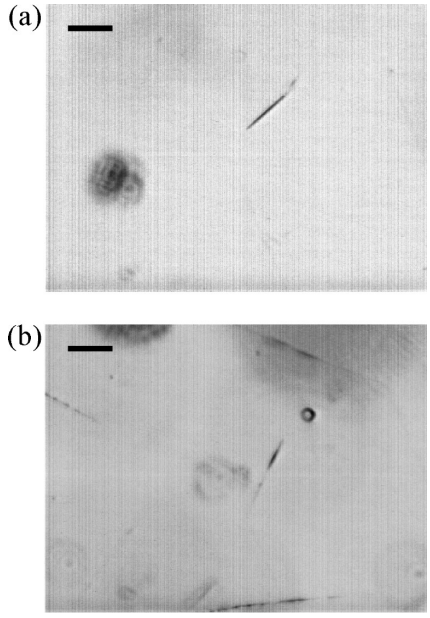

Figure 8. PVM images (scale bar 100 μm) from Run 2m at (a) 41 min, at first detection of monohydrate crystals, (b) 52 min, at the onset of an increase in the particle counts/s.

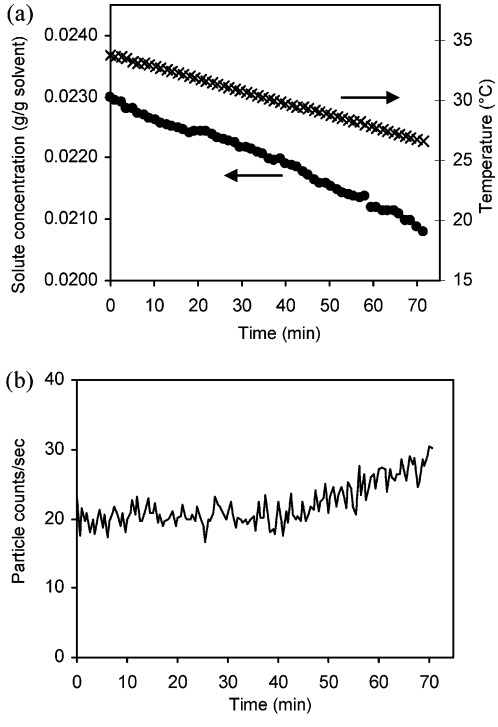

Figure 9. Run 4m experimental profiles with seeding at 0 min: (a) solute concentration and temperature, (b) particle counts/s.

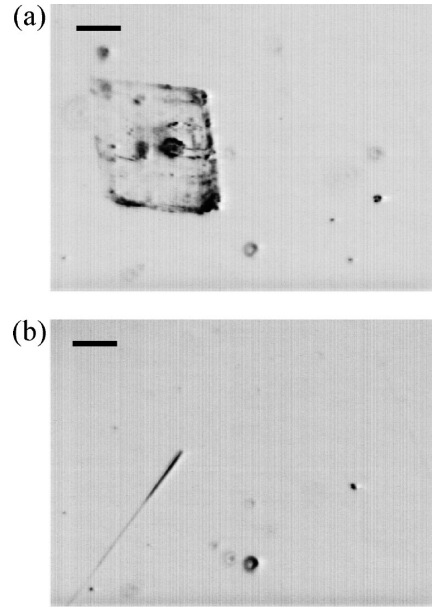

Figure 10. PVM images (scale bar 100 μm) from Run 4m at (a) 43 min, at the onset of an increase in particle counts/s, (b) 63 min, at first detection of monohydrate crystals.

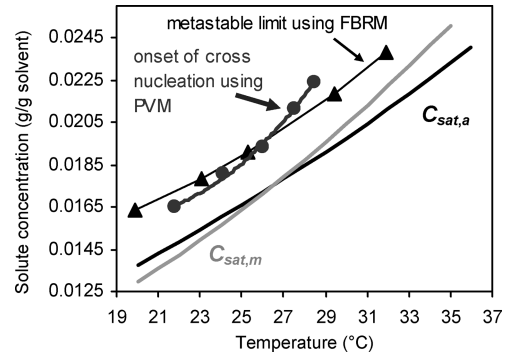

Figure 11. L-Phe solubility and seeded metastable limits.

form was evaluated using two methods: equilibrated slurries at isothermal conditions (similar to that for the anhydrate form) and subjected to slow heating. Previous solubility studies using slurries of monohydrate L-Phe crystals in water[31] reported significant solid-phase interference on the IR measurements leading to excessively higher and erroneous solute concentration predictions. This was likely due to the dimensions of the monohydrate crystals which were comparable to the penetration depth of the IR energy field ($\approx$1.0−2.0 μm, in that study). In the water/2-propanol system data reported in Figure 6, the interference on the IR measurements was not significant as verified by the identical solubility results obtained using the second method in which the equilibrium solute concentration was measured at the point of complete dissolution. Solid-form interference could become significant at much higher solids density[41] than occurred in the experiments in this study. Compared to L-Phe in water, a decrease in the transition temperature from 37.0[13,44] to 26.5 °C was observed in the mixed solvent. This was also reported for L-serine (in water−methanol solutions),[45] which has similar pseudo-dimorph behavior. The decrease in the transition temperature was attributed to a relatively larger increase in the heat of dissolution of the monohydrate form compared to that of the anhydrate form with the addition of methanol in the solvent.

The seeded metastable limit was determined using FBRM to detect secondary nucleation and in situ video microscopy to

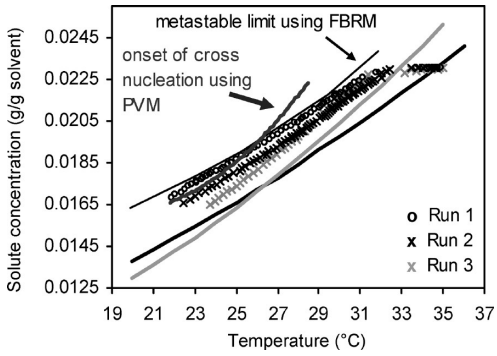

Figure 12. Supersaturation profiles implemented in the seeded batch crystallization runs.

identify the nucleated form. At temperatures below the transition point, for example in Run 2m, monohydrate needles were observed at 41 min, which was before an increase in particle counts/s at 52 min (see Figures 7and 8). The first limit determined via PVM images represents the onset of cross nucleation. Noise in the FBRM measurements resulted in its later detection of nucleation (Figure 7b). Above the transition point, for example, in Run 4m, needles were not detected prior to or at the onset of an increase in particle counts/s at 43 min (see Figures 9 and 10) but were only observed at a later time (at 63 min); this indicates that the nucleation detected via FBRM was that of the seeded anhydrate form. Unlike the monohydrate form, the anhydrate form was not easily detected using PVM until after its detection via FBRM, most likely due to the low number density of the nucleated crystals of the anhydrate form.

The seeded metastable limits associated with both types of secondary nucleation (both induced by the presence of anhydrate seed crystals; see Figure 11) provides an estimate of the maximum allowable supersaturation for the controlled growth of the anhydrate seed crystals, to avoid cross nucleation, which would impact the polymorph purity, and avoid nucleation of the seeded form, which would affect the crystal size distribution of the anhydrate-form product.

Concentration-Controlled Batch Crystallization. Three seeded crystallization experiments at various supersaturation profiles were implemented with concentration feedback control (Figure 12). Run 1 was implemented at a constant supersaturation ($\Delta C_a = 0.00200$ g/g of solvent) that was very close to the metastable limit determined using FBRM while exceeding the metastable limit for cross nucleation determined using PVM. The increase in the particle counts/s (Figure 13b), which starts at 36 min at about 30.3 °C, was attributed to the nucleation of the anhydrate form since the monohydrate needles were not detected via PVM images until about 104 min at about 28.5 °C (Figure 14). The appearance of the needles at 28.5 °C even though the supersaturation profile did not cross the metastable limit for cross nucleation at this point was likely

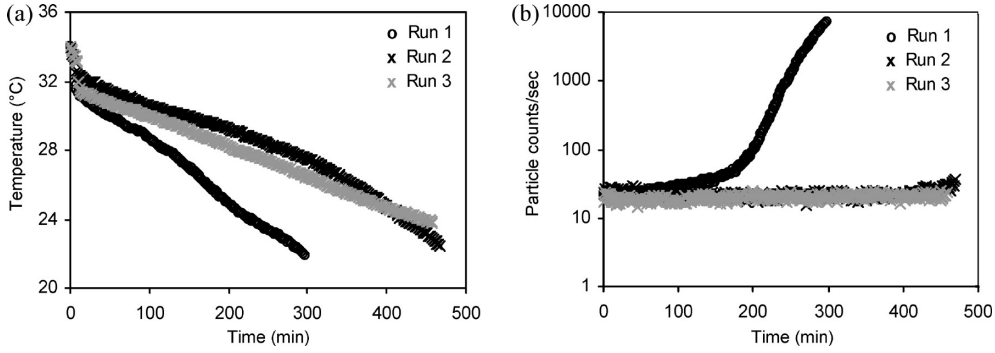

Figure 13. Experimental profiles in the seeded batch crystallization runs (with seeding at 0 min): (a) temperature, (b) particle counts/s.

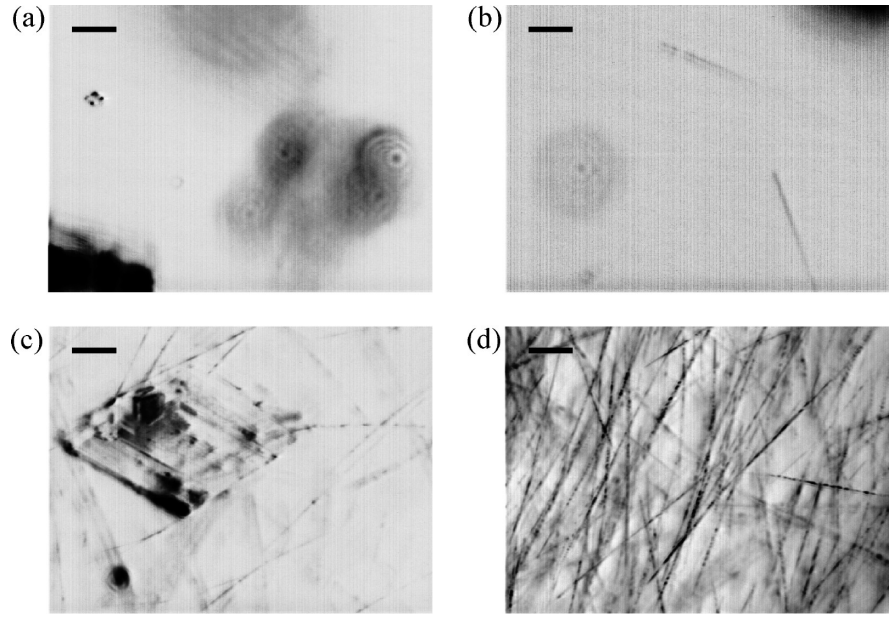

Figure 14. PVM images (scale bar 100 μm) from Run 1 at (a) 36 min, at the onset of an increase in particle counts/s, (b) 104 min, at first detection of monohydrate crystals, (c) 243 min, (d) 296 min.

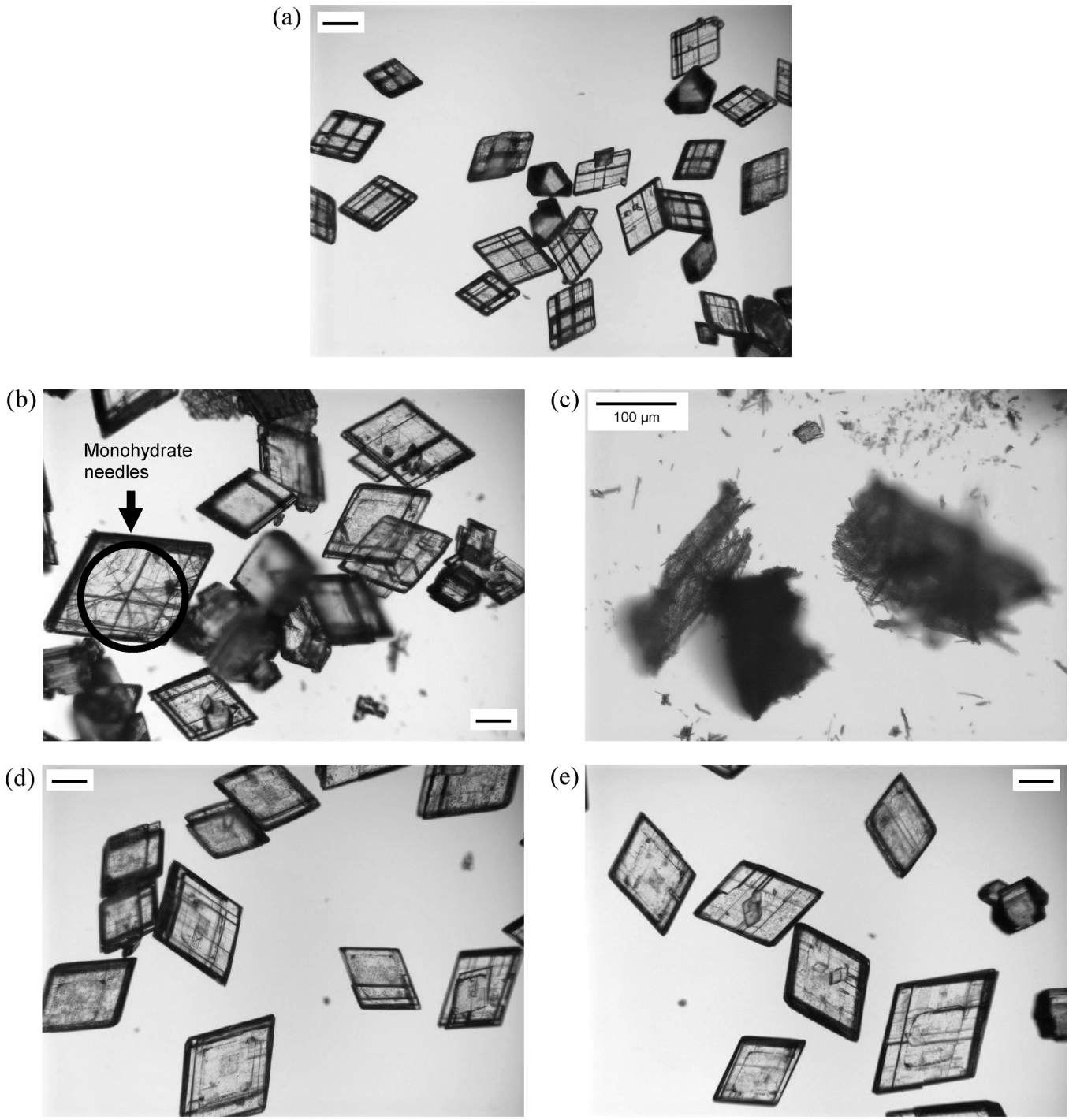

Figure 15. Microscopy images of seed and product crystals (scale bar 200 μm, unless stated otherwise): (a) seeds - anhydrate form, (b) Run 1 products - monohydrate form crystals observed on the anhydrate crystal surfaces, (c) Run 1 products - agglomerates of monohydrate form crystals, (d) Run 2 products - anhydrate form, (e) Run 3 products - anhydrate form.

due to increased surface area (and hence higher overall cross nucleation rate). Microscopy images of the seed (Figure 15a) and product crystals from Run 1 (Figure 15b,c) show that the needles agglomerated upon filtration (Figure 15c), such that individual needles were not well dispersed in the dried product sample compared to the slurry. The needles were observed on anhydrate crystal surfaces (Figure 15b) while anhydrate crystals smaller than the seed size were also detected (Figure 16). The amount of the monohydrate form in the product crystals estimated from PXRD (Figure 17) was about 9 wt % (Table 5).

Run 2 was implemented with a smaller constant supersaturation ($\Delta C_a = 0.00150$ g/g of solvent), which was within the metastable limits throughout the run (Figure 12). The particle counts/s profile (see Figure 12, 13b) showed a slight increase towards the end at 381 min (at 25.3 °C). The supersaturation profile was near the metastable limit for cross nucleation, which suggested that the cause of the increase was cross nucleation. A small number of monohydrate needles was detected in the PVM images (Figure 12, 18b) prior to this at 291 min (at about 27.6 °C). The initial number of needles nucleated was sufficiently low such that it took ~90 min before cross nucleation was substantial enough to be detected by FBRM. Figure 15d shows the product crystals of this run, which consisted of anhydrate crystals of more uniform size (Figure 12, 16). The

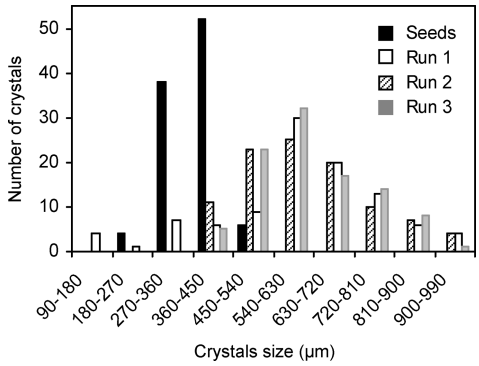

Figure 16. Size distributions of 100 L-Phe anhydrate seed and product crystals (based on the largest diagonal length measurable from microscopy images).

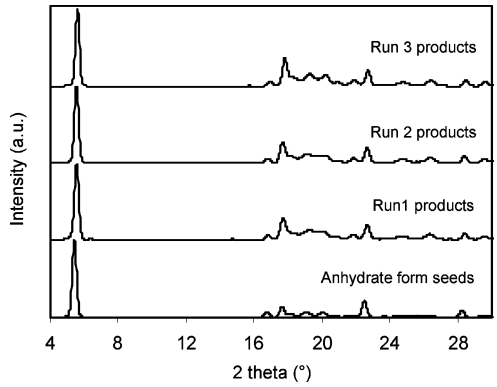

Figure 17. PXRD patterns of seed and product crystals.

Table 5. PXRD Analysis of Seed and Product Crystals

sample	estimated solid composition (wt% monohydrate, ±1.81)[a]
seeds	1.09, 0.00; average = 0.55
Run 1 products	8.03, 10.86; average = 9.45
Run 2 products	1.06, 0.00; average = 0.53
Run 3 products	0.00, 1.14; average = 0.57

[a] Based on 95% confidence interval.

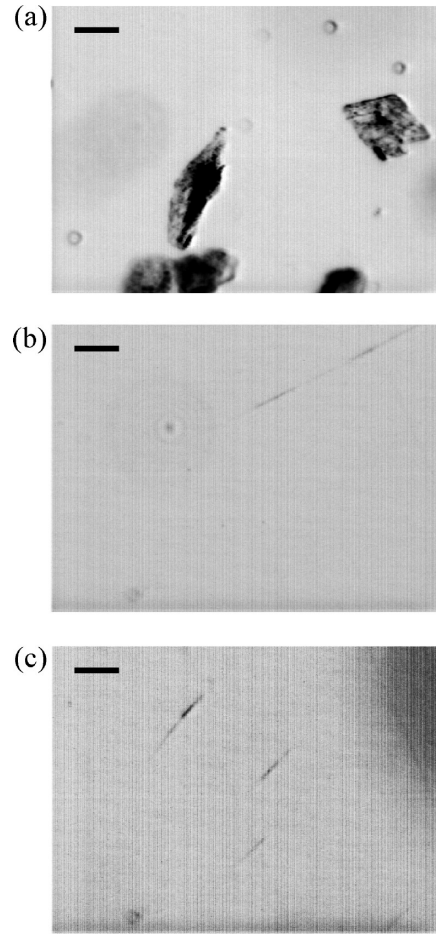

Figure 18. PVM images (scale bar 100 μm) from Run 2 at (a) 40 min, (b) 291 min, at first detection of monohydrate crystals, (c) 381 min, at onset of an increase in particle counts/s.

monohydrate needles, however, were not readily observed in the microscopy images, and the characteristic peaks of this form were also absent in the PXRD pattern of the product crystals (Figure 12, 17). Cross nucleation, although detected in situ, did not produce a large enough mass of the monohydrate needles to be detected by PXRD.

A disadvantage of the recipes in Runs 1 and 2 was that, by keeping the supersaturation with respect to the anhydrate form constant, the supersaturation with respect to the monohydrate was slowly increasing. This provided an increasing tendency for cross nucleation as the experiment progressed. A better approach to prevent cross nucleation is to maintain a low supersaturation with respect to the monohydrate form while growing the anhydrate form. Run 3 was implemented with constant supersaturation with respect to the monohydrate solubility ($\Delta C_m = 0.00110$ g/g of solvent); this translated into a varying driving force for the anhydrate form ranging from approximately 0.00190 to 0.00070 g/g of solvent.

This recipe was selected such that the supersaturation was less than that of Run 1 from 30.3 °C onwards, to avoid secondary nucleation of the anhydrate form, and was below that of Run 2 from 27.6 °C onwards to prevent cross nucleation. This recipe was successful in preventing any significant cross nucleation as shown by the constant particle counts/s (Figure 13b) and the absence of the monohydrate needles in the PVM images (Figure 19) throughout the run. Run 3 provided the best batch recipe in terms of high polymorph purity (Table 5) and relatively narrower size distribution of the anhydrate-form products (Figures 15e and 16). Other means of selective crystallization, for example, using solvent-mediated transformation[46−50] of the metastable monohydrate form above the transition temperature (which was used to obtain the anhydrate seeds), led to a wider size distribution of the anhydrate crystals.

The cross nucleation detected in Runs 1 and 2, even though the supersaturation profiles did not cross the metastable limit for cross nucleation, suggests that the metastable limit described a practical upper bound of the operating regime in the initial stages of crystallization, but less so as the experiments progressed due to the effect of increasing crystal mass on promoting secondary nucleation. The cooling rate used in the initial stages (prior to seeding) in the batch crystallization runs was similar to that in the metastable limit experiments. However, upon seeding and starting concentration feedback control, the cooling rates (Figure 13a) ranged from 0.03−0.04, 0.02−0.03, and 0.02 °C/min for Runs 1, 2, and 3, respectively. As the experiment progressed, there was increasing dissimilarity in the operating conditions (specifically the mass of the solid phase and the cooling rate) between the metastable limit experiments and the concentration-controlled runs, and the upper bounds identified in the former were no longer representative of the actual conditions in the latter. Nonetheless, appropriate batch crystallization recipes can be designed systematically based on

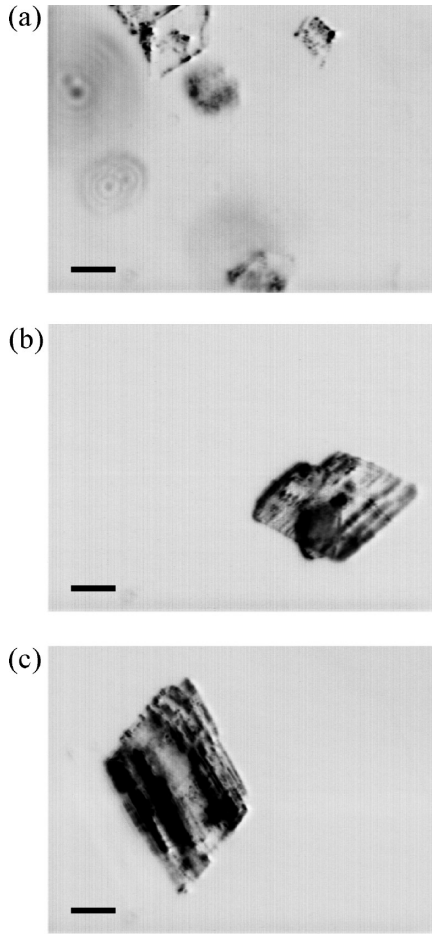

Figure 19. PVM images (scale bar 100 μm) from Run 3 at (a) 40 min, (b) 300 min, (c) 400 min.

constant ΔC_m and using the results of earlier ΔC_a recipes as a more appropriate indication of the upper bound to effectively prevent secondary nucleation in the later stages of the operation.

Conclusions

A batch recipe for the selective crystallization of the metastable anhydrate form of an enantiotropic pseudo-dimorph system, L-phenylalanine in a mixed solvent system (75 wt % water and 25 wt % 2-propanol), was identified as a desired trajectory in the phase diagram. The solubility curves of both pseudo-dimorphs were determined using ATR-FTIR spectroscopy combined with chemometrics. Laser backscattering was used to determine the seeded metastable limit, and the nucleated forms were identified using in situ video microscopy. Various preset supersaturation profiles were followed during crystallization using concentration feedback control to adjust the cooling rate accordingly based on in situ solute concentration measurements. Metastable limits determined to suppress uncontrolled secondary nucleation of either form defined the maximum allowable supersaturation for operations. Batch crystallization implemented at low constant absolute supersaturation with respect to the monohydrate form suppressed cross nucleation and was successful in selectively growing large anhydrate crystals of relatively uniform size to temperatures below the transition point, where the anhydrate form is metastable. Similar operations stopping above the transition temperature, where the anhydrate form is stable, would simplify preferentially growth of anhydrate crystals but would have reduced product yield. This methodology for the selective growth of metastable crystals extended the useful range of the phase diagram to increase product yield. This method is potentially applicable to other enantiotropic systems.

Acknowledgment. Mitsuko Fujiwara is acknowledged for providing technical advice on this project. The authors thank Scott Wilson and Maya Ramesh from the 3M Materials Laboratory at the University of Illinois for the PXRD data collection. The authors also thank Jim Mabon for the SEM imaging carried out in the Frederick Seitz Materials Research Laboratory Central Facilities, University of Illinois, which are partially supported by the U.S. Department of Energy under Grants DE-FG02-07ER46453 and DE-FG02-07ER46471.

References

(1) Davey, R. J.; Garside, J. *From Molecules to Crystallizers*; Oxford: Oxford University Press, 2000.
(2) Togkalidou, T.; Tung, H. H.; Sun, Y.; Andrews, A. T.; Braatz, R. D. *Ind. Eng. Chem. Res.* **2004**, *43*, 6168–6181.
(3) Worlitschek, J.; Mazzotti, M. *Cryst. Growth Des.* **2004**, *4*, 891–903.
(4) Chung, S. H.; Ma, D. L.; Braatz, R. D. *Chemom. Intell. Lab. Syst.* **2000**, *50*, 83–90.
(5) Garti, N.; Sarig, S.; Wellner, E. *Thermochim. Acta* **1980**, *37*, 131–136.
(6) Sato, K.; Suzuki, K.; Okada, M. *J. Cryst. Growth* **1985**, *72*, 699–704.
(7) Profir, V. M.; Rasmuson, A. C. *Cryst. Growth Des.* **2004**, *4*, 315–323.
(8) Mirmehrabi, M.; Rohani, S. *J. Pharm. Sci.* **2005**, *94*, 1560–1576.
(9) Trifkovic, M.; Rohani, S. *Org. Proc. Res. Dev.* **2007**, *11*, 138–143.
(10) Doki, N.; Yokota, M.; Kido, K.; Sasaki, S.; Kubota, N. *Cryst. Growth Des.* **2004**, *4*, 103–107.
(11) Doki, N.; Seki, H.; Takano, K.; Asatani, H.; Yokota, M.; Kubota, N. *Cryst. Growth Des.* **2004**, *4*, 949–953.
(12) Davey, R. J.; Blagden, N.; Potts, G. D.; Docherty, R. *J. Am. Chem. Soc.* **1997**, *119*, 1767–1772.
(13) Mohan, R.; Koo, K. K.; Strege, C.; Myerson, A. S. *Ind. Eng. Chem. Res.* **2001**, *40*, 6111–6117.
(14) Gracin, S.; Uusi-Penttila, M.; Rasmuson, A. C. *Cryst. Growth Des.* **2005**, *5*, 1787–1794.
(15) Yano, J.; Milhofer, H. F.; Wachtel, E.; Garti, N. *Langmuir* **2000**, *16*, 10005–10014.
(16) Fujiwara, M.; Nagy, Z. K.; Chew, J. W.; Braatz, R. D. *J. Proc. Control* **2005**, *15*, 493–504.
(17) Threlfall, T. *Org. Proc. Res. Dev.* **2000**, *4*, 384–390.
(18) Beckmann, W. *Org. Proc. Res. Dev.* **2000**, *4*, 372–383.
(19) Gracin, S.; Rasmuson, A. C. *Cryst. Growth Des.* **2004**, *4*, 1013–1023.
(20) Lin, S. W.; Ng, K. M.; Wibowo, C. *Ind. Eng. Chem. Res.* **2007**, *46*, 518–529.
(21) Lewiner, F.; Klein, J. P.; Fevotte, G. *Chem. Eng. Sci.* **2001**, *56*, 2069–2084.
(22) Sato, K.; Boistelle, R. *J. Colloid Interface Sci.* **1983**, *94*, 593–596.
(23) Threlfall, T. *Org. Proc. Res. Dev.* **2003**, *7*, 1017–1027.
(24) Feng, L. L.; Berglund, K. A. *Cryst. Growth Des.* **2002**, *2*, 449–452.
(25) Liotta, V.; Sabesan, V. *Org. Proc. Res. Dev.* **2004**, *8*, 488–494.
(26) Gron, H.; Borissova, A.; Roberts, K. J. *Ind. Eng. Chem. Res.* **2003**, *42*, 198–206.
(27) Fujiwara, M.; Chow, P.; Ma, D.; Braatz, R. D. *Cryst. Growth Des.* **2002**, *2*, 363–370.
(28) Zhou, G. X.; Fujiwara, M.; Woo, X. Y.; Rusli, E.; Tung, H. H.; Starbuck, C.; Davidson, O.; Ge, Z.; Braatz, R. D. *Cryst. Growth Des.* **2006**, *6*, 892–898.
(29) Nagy, Z. K.; Chew, J. W.; Fujiwara, M.; Braatz, R. D. *J. Proc. Control* **2008**, *18*, 399–407.
(30) Yu, Z. Q.; Chow, P. S.; Tan, R. B. H. *Ind. Eng. Chem. Res.* **2006**, *45*, 438–444.
(31) Kee, N. C. S. *PhD Thesis*, University of Illinois at Urbana-Champaign and National University of Singapore, 2008.
(32) Khawas, B. *Indian J. Phys.* **1985**, *59A*, 219–226.
(33) Workman, J. J.; Mobley, P.; Kowalski, B.; Bro, R. *Appl. Spec. Rev.* **1996**, *31*, 73–124.
(34) Mobley, P. R.; Kowalski, B. R.; Workman, J. J.; Bro, R. *Appl. Spec. Rev.* **1996**, *31*, 347–368.
(35) Tahti, T.; Louhi-Kultanen, M.; Palosaari, S. In *14th International Symposium on Industrial Crystallization*; Institution of Chemical Engineers: Rugby, UK, 1999; pp 1−9.

(36) Barrett, P.; Glennon, B. *Trans. Inst. Chem. Eng.* **2002**, *80*, 799–805.
(37) Togkalidou, T.; Fujiwara, M.; Patel, S.; Braatz, R. D. *J. Cryst. Growth* **2001**, *231*, 534–543.
(38) Togkalidou, T.; Braatz, R. D.; Johnson, B. K.; Davidson, O.; Andrews, A. *AIChE J.* **2001**, *47*, 160–168.
(39) Togkalidou, T.; Tung, H. H.; Sun, T. K.; Andrews, A.; Braatz, R. D. *Org. Proc. Res. Dev.* **2002**, *6*, 317–322.
(40) Xie, Y.; Kalivas, J. *Anal. Chim. Acta* **1997**, *348*, 19–27.
(41) O'Sullivan, B. Ph.D. Thesis, University College Dublin: Dublin, Ireland, 2005.
(42) Dunuwila, D. D.; Carroll, L. B.; Berglund, K. A. *J. Cryst. Growth* **1994**, *137*, 561–568.
(43) Nyvlt, J.; Sohnel. O.; Matuchova, M.; Broul, M. *The Kinetics of Industrial Crystallization*; Elsevier: New York, 1985.
(44) Sato, T.; Sano, C. European Patent #0703214A2, 1995.
(45) Luk, J. C.; Rousseau, R. W. *Cryst. Growth Des.* **2006**, *6*, 1808−1812.
(46) Maruyama, S.; Ooshima, H.; Kato, J. *Chem. Eng. J.* **1999**, *75*, 193–200.
(47) Starbuck, C.; Spartalis, A.; Wai, L.; Jian, W.; Fernandez, P.; Lindemann, C. M.; Zhou, G. X.; Ge, Z. *Cryst. Growth Des.* **2002**, *2*, 515–522.
(48) Hu, Y.; Liang, J. K.; Myerson, A. S.; Taylor, L. S. *Ind. Eng. Chem. Res.* **2005**, *44*, 1233–1240.
(49) Qu, H.; Louhi-Kultanen, M.; Rantanen, J.; Kallas, J. *Cryst. Growth Des.* **2006**, *6*, 2053–2060.
(50) Caillet, A.; Puel, F.; Fevotte, G. *Int. J. Pharm.* **2006**, *307*, 201–208.
(51) Kim, K.-J.; Mersmann, A. *Chem. Eng. Sci.* **2001**, *56*, 2315–2324.

CG8006537